The effect of resistive forces in variable recruitment fluidic artificial muscle bundles: a configuration study

Mazzoleni, Nicholas, Kim, Jeong Yong, Bryant, Matthew

Nicholas Mazzoleni, Jeong Yong Kim, Matthew Bryant, "The effect of resistive forces in variable recruitment fluidic artificial muscle bundles: a configuration study," Proc. SPIE 11374, Bioinspiration, Biomimetics, and Bioreplication X, 113740J (20 May 2020); doi: 10.1117/12.2557907

SPIE.

Event: SPIE Smart Structures + Nondestructive Evaluation, 2020, Online Only

The Effect of Resistive Forces in Variable Recruitment Fluidic Artificial Muscle Bundles: A Configuration Study

Nicholas Mazzoleni[a], Jeong Yong Kim[a], Matthew Bryant[a]
[a]North Carolina State University Department of Mechanical & Aerospace Engineering,
1840 Entrepreneur Dr., Raleigh, NC 27606

ABSTRACT

The use of soft, compliant actuators has recently gained research attention as a potential approach to improve human-robot interaction compatibility. Fluidic artificial muscles, or McKibben actuators, are a popular class of soft actuator due to their low cost and high force-to-weight ratio. However, traditional McKibben actuators face efficiency problems, as in most actuation schemes, the actuator is sized for the largest possible load, resulting in energy loss when operating at lower force regimes. To address this issue, our group has developed a bio-inspired actuation strategy called variable recruitment. In variable recruitment, actuators are placed within a bundle and can be sequentially activated depending on the required load. This strategy mimics the hierarchical architecture of mammalian muscle tissue and improves system efficiency and bandwidth while allowing for variable stiffness properties. Previous variable recruitment models and controllers assume that the force output of each actuator is independent and that these forces sum to provide the total bundle force. However, our recent work has shown that there is significant interaction between actuators within a bundle, particularly at lower recruitment states. This is because at these states, inactive or partially activated actuators resist bundle motion and reduce total force production. In this paper, we study these resistive effects at low recruitment states by considering two different variable recruitment configurations: a fixed-end configuration (with resistive forces) and a tendon configuration (designed with tendons to eliminate resistive forces). We then assess the tradeoffs between the two configurations. We found that while using the tendon configuration eliminates resistive forces, if we consider both configurations with the same overall system length, the tendon configuration has less overall system free strain because its FAMs have to be shorter than those of the fixed-end configuration. However, despite this difference in free strain, our results still show that the tendon configuration can have higher maximum load capacity and efficiency than the fixed-end configuration and that the specific application and system requirements will dictate the proper configuration choice.

Keywords: Fluidic artificial muscles, variable recruitment, inactive/partially activated motor units, resistive forces

1. INTRODUCTION

Fluidic artificial muscles, known by some as McKibben actuators, were invented by Joseph McKibben in the 1960s to help his daughter, who suffered from polio.[1] A fluidic artificial muscle (FAM) consists of an elastomeric bladder surrounded by a braided sheath. When the bladder is filled with a working fluid (hydraulic or pneumatic), it radially expands, and the geometric constraints imposed by the braided sheath cause the muscle to axially contract. Although FAMs have been around for many decades, they have received increased attention in recent years due to advancements in robotics and the desire for soft, compliant, and safe actuation in mobile robotics. FAMs are a logical choice of soft actuator due to their low cost, ease of manufacturability, and high force-to-weight ratio. While FAMs were originally pneumatically actuated, recent work has shown that significant efficiency gains can be made if a hydraulic working fluid is used due to the incompressibility of the fluid.[2] This has led researchers to investigate other ways to increase the efficiency of FAM-actuated systems, which has resulted in the development of a variable recruitment actuation scheme. Whereas the size of conventional hydraulic systems (including FAM-based systems) is determined by the maximum required load, in variable recruitment, actuators are divided into bundles with discrete motor units, each of which can be activated separately based on the required load. This idea was inspired by mammalian muscle tissue physiology, in which muscle tissue motor units are sequentially activated to achieve tasks that require different force levels. These motor units are recruited from smallest to largest, which is known as Henneman's Size Principle.[3] By leveraging the concept of variable recruitment, we can increase system efficiency and performance. This is because in a single-actuator system, to achieve lower force regimes, the system pressure must be throttled, resulting in a significant loss of energy. However, in this multi-actuator variable recruitment system, lower force regimes can be achieved simply by sequentially activating individual motor units, requiring less throttling and increasing efficiency. Variable recruitment was first shown to be more efficient than a single

Bioinspiration, Biomimetics, and Bioreplication X, edited by Mato Knez, Akhlesh Lakhtakia, Raúl J. Martín-Palma,
Proc. of SPIE Vol. 11374, 113740J · © 2020 SPIE · CCC code: 0277-786X/20/$21 · doi: 10.1117/12.2557907

equivalent actuator in 2014 by Bryant et al.[4] Since then, experimental characterizations of variable recruitment bundles have demonstrated efficiency gains in both pneumatic and hydraulic systems,[5,6] while other analytical studies have developed real-time variable recruitment switching control schemes[7] and system-level models that demonstrate increased system efficiency and bandwidth improvements.[8]

Initial variable recruitment studies used simple idealized models that can be derived using a virtual work balance, shown succinctly by Tondu.[1] This ideal model captures many aspects of FAM force-strain behavior, but it does not predict pressure-dependent free contraction and also overpredicts blocked force. This model can be corrected using semi-empirical correction factors for a given actuator specimen as long as there is sufficient experimental data to properly characterize that actuator.[9] This corrected model helps to better match the blocked force and free strain of a given actuator, but due to its curve-fit nature, it cannot accurately predict forces for contractions beyond free strain (i.e. external compression of the FAM), when the actuator starts to contribute negative, or resistive, force.[10] Having knowledge of this resistive force is essential when analyzing a variable recruitment artificial muscle bundle because of the method in which additional motor units are brought online, which is called orderly recruitment.[7] The concept of orderly recruitment is most easily understood through example. Let us consider a bundle of three McKibben muscle actuators. Each actuator within the bundle comprises a single motor unit, and the pressure of each motor unit can be controlled independently through the use of a servo valve. In orderly recruitment, an increasing load initially causes the first motor unit to be activated (i.e. pressurized) while the others remain inactive (i.e. vented). If the activation of the first motor unit approaches saturation before the load demand is satisfied, activation level (pressure) is increased in the second motor unit while the third is maintained as inactive. This pattern continues until the load demand is satisfied, or until all motor units in the bundle are saturated at maximum pressure.

In traditionally-constructed experimental variable recruitment bundles, the inactive motor units will compress during orderly recruitment, providing a resistive force that decreases the overall tensile force output of the bundle.[4,11–15] If the contraction of the bundle is high enough, these inactive motor units will even buckle.[4,6,12,13] Additionally, due to the pressure-dependent free strain behavior of FAMs, partially-activated FAMs in a higher recruitment state will have lower free strain than fully-activated FAMs, resulting in resistive forces if the overall bundle strain exceeds the free strain of the partially activated FAMs. To perform an analytical study that captures these effects, we need a model that can account for both pressure-dependent free strain behavior and post-free strain behavior. Several models in the literature include this behavior in individual FAMs and use either the virtual work method[16,17] or a force balance method.[17–19] In this paper, we have chosen to use the model developed by Klute et al.[16] to serve as the foundation of an analytical study that studies resistive forces during orderly recruitment. Additional details and assumptions of this model will be discussed in the next section of this paper. We can address the issue of resistive forces in a few different ways, but in this paper, we will discuss how these forces can be mitigated through hardware design by attaching tendons to each FAM in the bundle to prevent compression. We will then discuss the tradeoffs associated with this particular hardware design and suggest opportunities for future study.

2. BUNDLE CONFIGURATIONS AND FORCE MODEL

2.1 'Fixed-end' Configuration vs. 'Tendon' Configuration

To date, the FAM bundles used in variable recruitment experiments have been in a 'fixed-end' configuration. In this configuration, the ends of the FAMs within the bundle are fixed to rigid endplates, with one endplate fixed to mechanical ground and one endplate connected to a movable load. To mitigate the resistive forces of inactive or partially activated FAMs, we can introduce flexible, yet inextensible, tendons into the system. These tendons will help inactive FAMs or partially activated FAMs that have already reached free strain remain uncompressed when the bundle contracts, ensuring that there is no resistive force. To compare the fixed-end and tendon configurations, let us consider a packaging design constraint, in which the overall length of the system must be the same regardless of which configuration is implemented. This is a realistic design constraint, because if, for example, the FAM bundle is used as a robotic limb, the bundle must fit within the predetermined physical limits of the robot. A sketch of the two configurations can be seen below. We can observe that for the fixed-end configuration, the length of the total system and the length of the individual FAMs is identical, while for the tendon configuration, the length of individual FAMs is shorter than overall system length, since the tendons occupy some of the available system length.

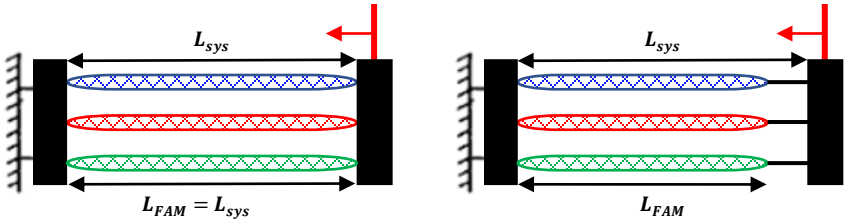

Figure 1. Side-by-side comparison of FAM bundle configurations. The fixed-end configuration (left) and tendon configuration (right) have the same total system length but different FAM lengths. Mechanical ground is indicated at the leftmost end of each picture and the direction of contraction is indicated by the red arrow.

A key design decision that must be made for the tendon configuration is the length of the tendons. The most general way to define tendon length is to impose the requirement that the bundle does not experience any resistive force from any of its FAMs throughout its entire range of contraction. To develop the mathematical formulation for this tendon length requirement, let us first define our total system strain:

$$\varepsilon_{sys} = \frac{\Delta L_{sys}}{L_{sys}} \tag{1}$$

where ΔL_{sys} is the total system displacement and L_{sys} is the initial total system length. We can relate FAM strain within a given configuration to total system strain through the following equation:

$$\varepsilon_{FAM} = \varepsilon_{sys}\left(\frac{L_{sys}}{L_{FAM}}\right) \tag{2}$$

where L_{FAM} is the initial length of FAMs within the bundle. This length is dependent on the length of the tendons. Using the condition that there must be no resistive forces throughout the entire range of contraction, we can define the tendon length as follows:

$$L_{ten} > L_{FAM}\varepsilon_{FAM,free} \tag{3}$$

We can relate the free strain of the FAMs within the bundle to the overall free strain through Equation 2 to get an expression for the maximum length of a FAM within the tendon configuration:

$$L_{FAM} \leq L_{sys}(1 - \varepsilon_{sys,free}) \tag{4}$$

This relationship allows us to properly size our bundle for the tendon configuration such that there are no resistive forces over the entire range of useful FAM contraction.

2.2 FAM Bundle Force Model – Klute et al. Formulation

To account for resistive forces in the fixed-end configuration, we use the Klute et al. formulation for the force-strain relationship of fluidic artificial muscles.[16] This model uses a virtual work method to obtain an actuator force relationship for a single actuator:

$$F = P\frac{dV}{dL} + V_b\frac{dW}{dL} \tag{5}$$

where P is the instantaneous pressure supplied to the actuator, V is the instantaneous actuator volume, L is the instantaneous actuator length, V_b is the bladder volume (which remains constant), and dW is the change in strain energy. The model uses a nonlinear elastic Mooney-Rivlin strain energy density function for the second term, which accounts for elastic energy storage in the bladder. If we neglect this term, we are left with the more recognizable ideal model. More details regarding the equations of this model can be found in the original paper presenting the model.[16] However, for the purpose of this analysis, we need only understand that by including the second term in this model, we can characterize pressure-dependent free strain and post-free strain behavior, which are two of the critical factors we need to model resistive forces in variable recruitment bundles. It is important to note that the Klute et al. model does not predict the point at which a compressed FAM will buckle, so we used experimental data to approximate this behavior. An example of this experimental data is shown in Figure 2. We used this approximation to modify the Klute et al. model, which tends to overpredict forces past

the buckling point of FAMs. With the approximation, once the buckling point is reach, the resistive force no longer increases, but instead remains constant, allowing for a better characterization of the post-buckled force.

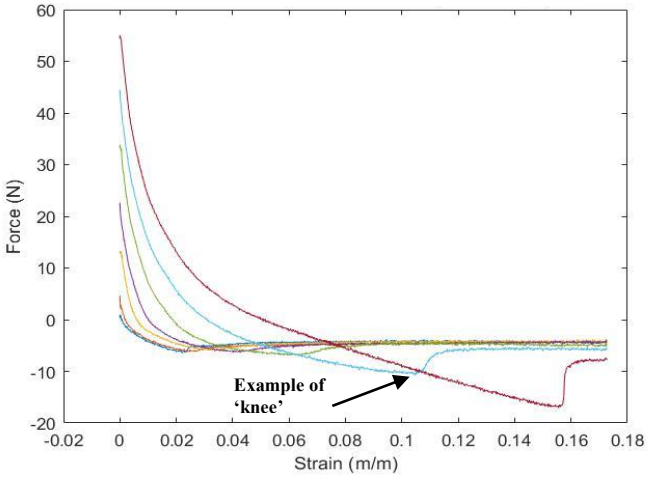

Figure 2. Sample experimental force-strain data for low-pressure FAMs (0-82.74 kPa). We used the location of the post-buckled 'knee' for each pressure to develop a curve-fit for the strain at which this knee occurs. Then, we modified the Klute et al. model so that the resistive force is constant after reaching this 'knee' point for all pressures between 0 and 82.74 kPa. This prevents the model from overpredicting the resistive force after buckling.

Let us now consider the example of a variable recruitment bundle consisting of 3 FAMs divided into 3 distinct motor units. In general, the overall force exerted by a bundle of FAMs is given by the following equation:

$$F_{bun}(P,\varepsilon) = \sum_{i=1}^{3} F_{MU,i}\,(P,\varepsilon) \tag{6}$$

where $F_{MU,i}$ is the total force exerted by the i^{th} motor unit. As each new motor unit is recruited, the bundle enters a new recruitment state. For example, the recruitment state in which both motor units 1 and 2 receive nonzero pressure is called the second recruitment state. In the first recruitment state of this example bundle, the inactive motor units of the second and third recruitment states contribute resistive forces to overall bundle force output. In the second recruitment state, the inactive motor unit from the third recruitment state contributes resistive forces. In previous variable recruitment models, these resistive forces from inactive motor units have been assumed to be equal to 0. However, we can now use the results of the Klute et al. formulation to calculate the resistive forces exerted by these inactive elements. In addition, if for any given recruitment state *i*, if the pressure of the i^{th} motor unit is less than maximum system pressure, then this recruitment state would be at *partial activation.* Previous models that account for pressure-dependent free strain have assumed that for a given recruitment state containing a partially activated motor unit, if the system strain exceeds the free strain of the partially active motor unit, then that motor unit contributes zero force to the bundle. However, in reality, when this happens, that motor unit actually contributes resistive force to the bundle. We can again use the Klute et al. model to calculate this resistive force and give a more accurate representation of force in a bundle containing partially activated motor units. We can still use Equation (*6* to calculate the overall bundle force, but now we have to consider the resistive forces at during the different activation levels of each recruitment state. For the tendon configuration, we do not have to consider the effect of resistive forces if the tendons are sized properly. Instead, we can consider the force exerted by any motor units that are not in tension to be equal to 0. Below, we can see representative plots of force vs. system strain for both bundle configurations for the same total system length.

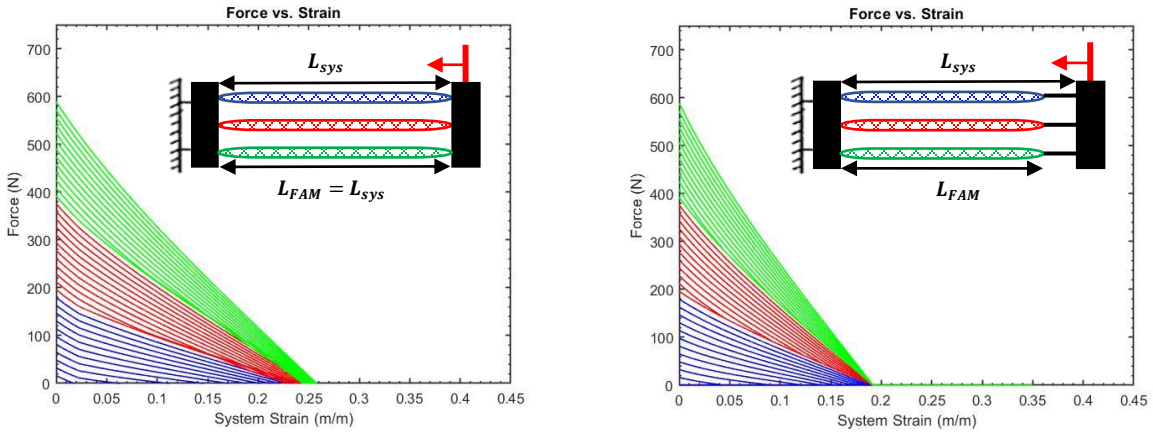

Figure 3. Plots of force vs. system strain for fixed-end configuration (left) and tendon configuration (right). FAMs in bundle had an initial length of 150 mm, initial radius of 6.35 mm, and initial braid angle of 33 degrees; plots were generated for a pressure range of 0 to 413.69 kPa (60 psi). The colors in the plots respond the first, second, and third recruitment states. Bundle force increases with increasing recruitment state.

From the plots, we see that in the fixed-end configuration, the maximum bundle free strain is pressure-dependent due to the resistive forces present in the lower recruitment states, while for the tendon configuration, the maximum bundle free strain is the same for each recruitment state. More importantly, we see that because the FAMs in the tendon configuration must be shorter to ensure no resistive force, the overall system free strain is less. This immediately demonstrates a tradeoff between the configurations, which we will explore further and quantify through an analysis of bundle efficiency and maximum load capacity.

3. COMPARISON OF EFFICIENCY AND MAXIMUM LOAD CAPACITY

3.1 System Efficiency Formulation

We next consider the actuation efficiency of a FAM bundle quasistatically lifting a constant load against gravity to a given desired system strain, as proposed by Meller et al.[6] Consider a mass m attached to the bundle, as shown in Figure 3. The work required to lift the mass to a desired system strain is given by:

$$W_{out} = mgL_{sys}\varepsilon_{sys,des} \tag{7}$$

where L_{sys} is initial total length of the actuator system and $\varepsilon_{sys,des}$ is the desired system strain. The total fluid energy input into the system is:

$$E_{in} = P_s \Delta V_{RS,i} \tag{8}$$

where P_s is maximum system pressure and $\Delta V_{RS,i}$ is the volume change associated with contraction to the desired system strain in the i^{th} recruitment state (consisting of n identically sized actuators), which is given by the following expression:

$$\Delta V_{RS,i} = ni \cdot \pi r_{0,i}^2 L_{sys}\left[\frac{(1-\varepsilon_{sys,des})}{sin^2\alpha_{0,i}} - \frac{(1-\varepsilon_{sys,des})^3}{tan^2\alpha_{0,i}}\right] \tag{9}$$

where $\alpha_{0,i}$, $r_{0,i}$, and L_{sys} are the initial braid angle, initial radius, and initial length, respectively, of the FAMs in the i^{th} recruitment state. Using these equations, we can calculate the efficiency for any given load:

$$\eta = \frac{W_{out}}{E_{in}} \tag{10}$$

We can then calculate efficiency over a wide range of loads. We use our FAM variable recruitment force-strain space to determine when a new recruitment state must be activated. The result of these efficiency calculations is a 'sawtooth' efficiency plot, as shown in Figure 3.

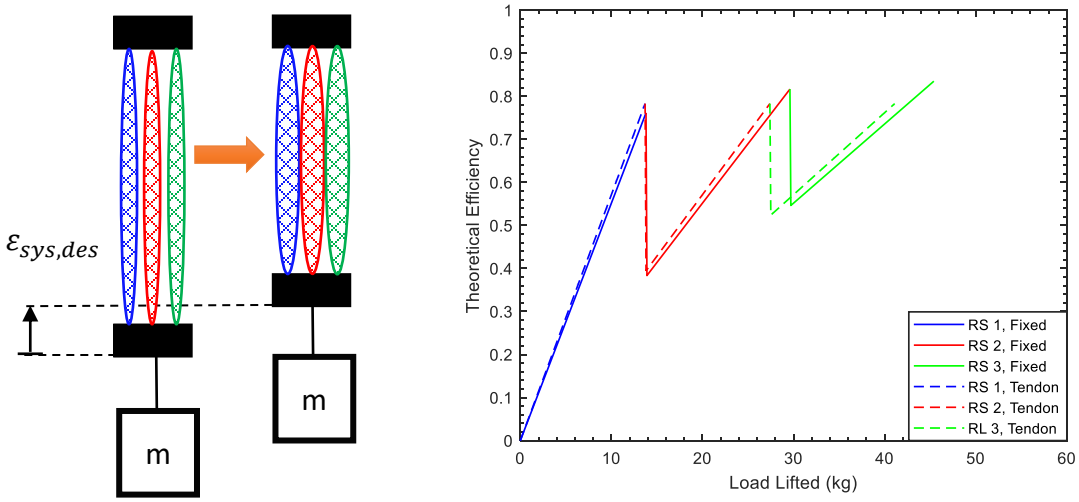

Figure 4. Loading scenario for efficiency calculation (left) and 'sawtooth' efficiency plot for a range of loads lifted for a desired system strain of 0.05. Recruitment state switching is determined using the force-strain space of a particular bundle.

3.2 Maximum Load Capacity and Efficiency Comparison

Now that we have defined our loading scenario for studying system efficiency, we can apply this analysis to our two configurations and compare them. Figure 5 shows a contour plot that visualizes the efficiency of each configuration as a function of desired system strain and load lifted. If we were to draw a vertical line that starts from any point on the horizontal axis and extend upward, we would trace out one of the individual sawtooth efficiency plots for a given desired system strain (as shown in Figure 4). From these plots, we can see that the maximum load lifted for the tendon configuration considerably decreases as we increase desired system strain. This is due to the reduction in system free strain due to the presence of a tendon within the configuration.

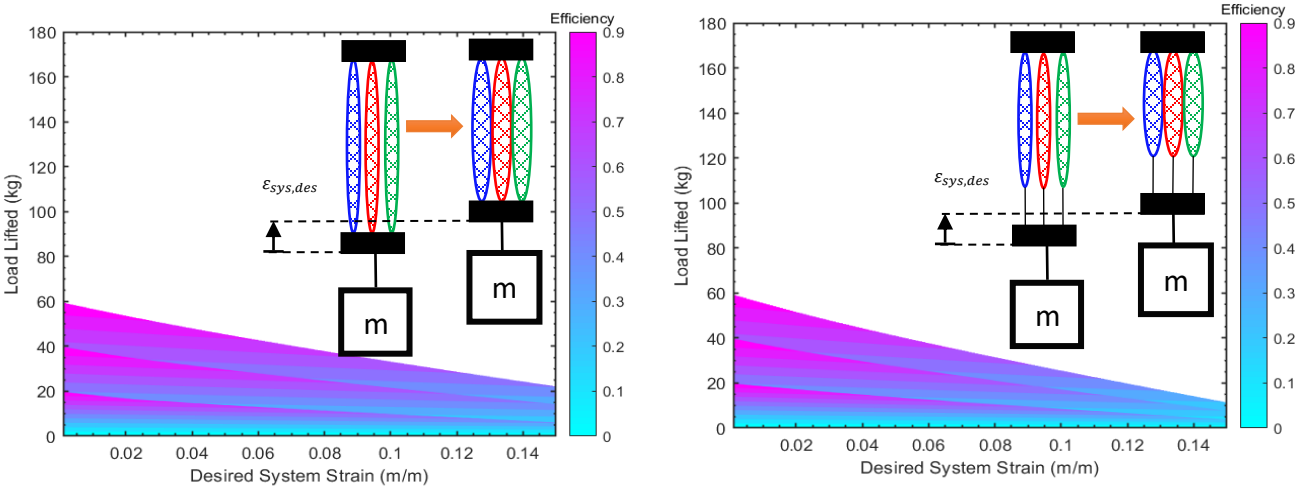

Figure 5. Contour efficiency plots for fixed-end configuration (left) and tendon configuration (right). Plots show efficiency as a function of load lifted and desired system strain.

These contour plots provide a good overview of efficiency over the entire operation space, but it can be difficult to discern specific trends in efficiency and maximum load capacity. Figure 6 shows the maximum load capacity and maximum efficiency associated with each recruitment state as a function of desired system strain. Maximum load capacity is the maximum load that can be lifted in a given recruitment state before the second recruitment state must be activated, while maximum efficiency is the efficiency value associated with this maximum load.

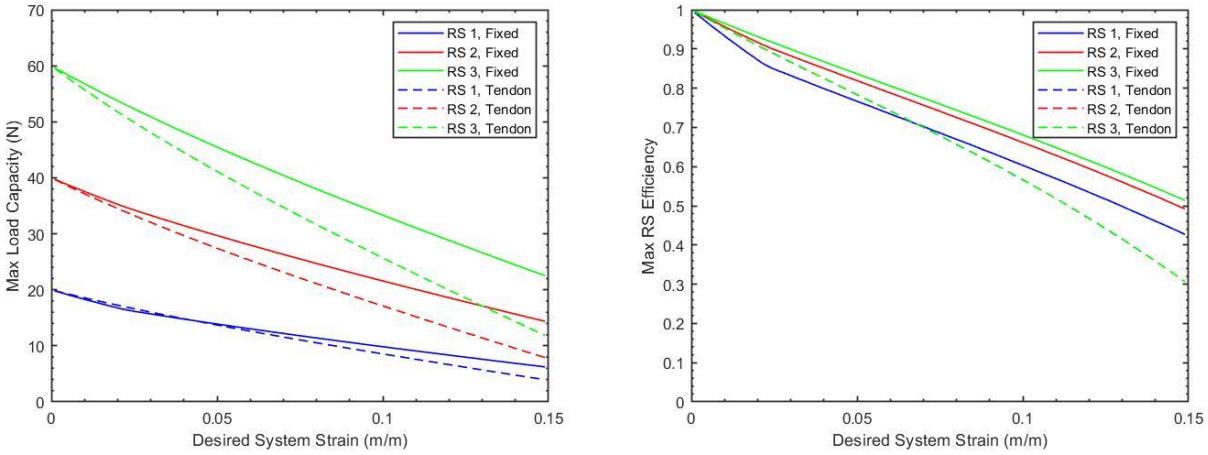

Figure 6. Plot of maximum load capacity vs. desired system strain (left) and maximum efficiency vs. desired system strain (right) for both configurations at all three recruitment levels. We can see the efficiency tradeoff associated with the difference in configuration, as a crossover between the two configurations occurs around a desired system strain of 0.07.

From these plots, we observe that maximum load capacity for the fixed-end configuration is greater than that of the tendon configuration for the entire range of desired system strains. By contrast, although the maximum efficiency for the fixed-end configuration is greater than that of the tendon configuration for recruitment states 2 and 3 for the entire range of desired system strains, for recruitment state 1, there is a range of desired system strains for which the tendon configuration is favorable. This illustrates that efficiency tradeoffs do exist due to the presence of resistive forces at lower recruitment states in the fixed-end configuration and lower system free strain in the tendon configuration. We can also compare the maximum efficiency for each recruitment state with the mean efficiency for each recruitment state, as shown below.

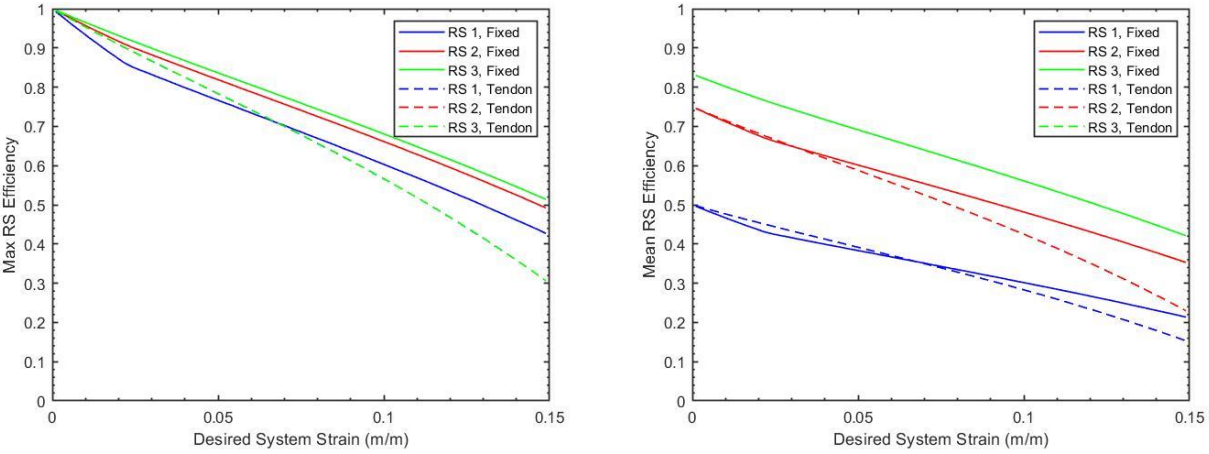

Figure 7. Plot of maximum recruitment state efficiency vs. desired system strain (left) compared with a plot of mean recruitment state efficiency vs. desired system strain (right).

When examining the mean efficiency plot, we see that the configuration trends are the same for recruitment states 1 and 2, but for recruitment state 3, the tendon configuration and fixed-end configuration have the same mean efficiency. This demonstrates that tradeoffs exist regardless of whether mean recruitment state efficiency or maximum recruitment state efficiency is used as an evaluation metric.

3.3 Other Considerations – *a priori* knowledge of desired system strain

Up to this point, we have sized the tendons in the tendon configuration such that the bundle experiences no resistive forces throughout the entire range of its contraction. Let us now consider the scenario in which we know the maximum desired

system strain *a priori*. Such a scenario might occur in an industrial robotics application, where a robot may be required to repeat the same prescribed task for thousands of cycles. In this scenario, our tendons could be sized such that the bundle experiences no resistive forces up to the point of maximum desired strain, and since contraction will not occur past this point, further tendon length is not required. Figure 7 shows the maximum load capacity and mean recruitment state efficiency for both configurations under this new requirement.

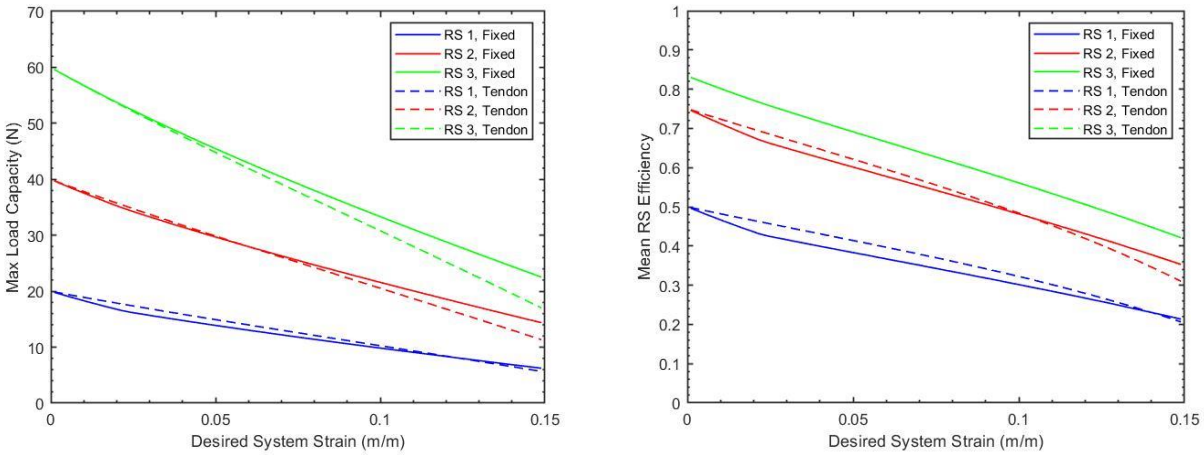

Figure 8. Plot of maximum load capacity vs. desired system strain (left) and mean recruitment state efficiency vs. desired system strain (right) when the maximum desired system strain is known *a priori*.

When we know the maximum desired system strain *a priori,* the performance of the tendon configuration improves because the tendons are shorter, allowing for longer FAMs and thus higher system free strain. We now observe that the tendon configuration performs better over almost the entire range of desired system strains for recruitment state 1, and there is now a mean efficiency crossover point for recruitment state 2. The implication of this result is that for a given application, there is an optimal tendon length that can be employed for a variable recruitment bundle that results in both better maximum load capacity and mean efficiency in lower recruitment states.

4. CONCLUSION AND FUTURE WORK

In this paper, we developed a model for a variable recruitment fluidic artificial muscle bundle that incorporates the effect of resistive forces due to inactive or partially activated motor units within different recruitment states. We then investigated a possible method to mitigate resistive forces in a bundle by attaching tendons to each FAM to prevent compression of inactive and partially activated FAMs at lower recruitment states. We compared this tendon configuration to the more traditional 'fixed-end' configuration by imposing a maximum system length constraint. The results of our study show that FAM bundles in the tendon configuration have lower overall system free strain than the fixed-end configuration, since the FAMs have to be shorter in the presence of the tendon. This leads to lower maximum load capacity than the fixed-end configuration; however, it does improve the efficiency of the bundle in recruitment state 1 at lower desired system strains. We also found that if the desired system strain is known *a priori* for a specific application, the tendon configuration performance is greatly improved because FAMs can be longer, providing more total system free strain. The primary purpose of this paper was to illustrate that certain tradeoffs exist between the configurations, and that the decision of which configuration to use must be made based on the application and system requirements. For future work, we would like to investigate 'mixed' configurations, where some FAMs have tendons and some do not. We would also like to experimentally validate the analytical results from this paper and develop criteria for optimal bundle design and recruitment state transitions based on a desired objective or system requirement.

5. ACKNOWLEDGEMENTS

The authors gratefully acknowledge funding support for this research from the National Science Foundation under Award No. CMMI-1845203 and Program Officer Irina Dolinskaya, as well as the NSF Graduate Research Fellowship Program.

REFERENCES

[1] Tondu, B., "Modelling of the McKibben artificial muscle: A review," Article Journal of Intelligent Material Systems and Structures **23**(3), 225–253.

[2] Tiwari, R., Meller, M. A., Wajcs, K. B., Moses, C., Reveles, I. and Garcia, E., "Hydraulic artificial muscles," Journal of Intelligent Material Systems and Structures **23**(3), 301–312 (2012).

[3] Henneman, E., Somjen, G. and Carpenter, D. O., "Excitability and inhibitability of motoneurons of different sizes," Journal of neurophysiology **28**(3), 599–620 (1965).

[4] Bryant, M., Meller, M. A. and Garcia, E., "Variable recruitment fluidic artificial muscles: modeling and experiments," Smart Materials and Structures **23**(7), 074009 (2014).

[5] DeLaHunt, S. A., Pillsbury, T. E. and Wereley, N. M., "Variable recruitment in bundles of miniature pneumatic artificial muscles," Bioinspiration & Biomimetics **11**(5), 056014 (2016).

[6] Meller, M., Chipka, J., Volkov, A., Bryant, M. and Garcia, E., "Improving actuation efficiency through variable recruitment hydraulic McKibben muscles: modeling, orderly recruitment control, and experiments," Bioinspiration & Biomimetics **11**(6), 065004 (2016).

[7] Jenkins, T. E., Chapman, E. M. and Bryant, M., "Bio-inspired online variable recruitment control of fluidic artificial muscles," Smart Materials and Structures **25**(12), 125016 (2016).

[8] Chapman, E., Jenkins, T. and Bryant, M., "Parametric Study of a Fluidic Artificial Muscle Actuated Electrohydraulic System," Volume 2: Modeling, Simulation and Control; Bio-Inspired Smart Materials and Systems; Energy Harvesting, V002T06A003, ASME (2016).

[9] Meller, M. A., Bryant, M. and Garcia, E., "Reconsidering the McKibben muscle: Energetics, operating fluid, and bladder material," Special Issue Article Journal of Intelligent Material Systems and Structures **25**(18), 2276–2293 (2014).

[10] Kim, J. Y., Mazzoleni, N. and Bryant, M., "Investigation of Resistive Forces in Variable Recruitment Fluidic Artificial Muscle Bundles," Proceedings of the 38th IMAC, A Conference and Exposition on Structural Dynamics 2020 (2020).

[11] Meller, M., Chipka, J., Volkov, A., Bryant, M. and Garcia, E., "Improving actuation efficiency through variable recruitment hydraulic McKibben muscles: modeling, orderly recruitment control, and experiments," Bioinspiration & Biomimetics **11**(6), 065004 (2016).

[12] Robinson, R. M., Kothera, C. S. and Wereley, N. M., "Variable Recruitment Testing of Pneumatic Artificial Muscles for Robotic Manipulators," IEEE/ASME Transactions on Mechatronics **20**(4), 1642–1652 (2015).

[13] DeLaHunt, S. A., Pillsbury, T. E. and Wereley, N. M., "Variable recruitment in bundles of miniature pneumatic artificial muscles," Bioinspiration & Biomimetics **11**(5), 056014 (2016).

[14] Chipka, J., Meller, M. A., Volkov, A., Bryant, M. and Garcia, E., "Linear dynamometer testing of hydraulic artificial muscles with variable recruitment," Original Article Journal of Intelligent Material Systems and Structures **28**(15), 2051–2063 (2017).

[15] Meller, M., Kogan, B., Bryant, M. and Garcia, E., "Model-based feedforward and cascade control of hydraulic McKibben muscles," Sensors and Actuators, A: Physical (2018).

[16] Klute, G. K. and Hannaford, B., "Accounting for elastic energy storage in mckibben artificial muscle actuators," Journal of Dynamic Systems, Measurement and Control, Transactions of the ASME **122**(2), 386–388 (2000).

[17] Kothera, C. S., Jangid, M., Sirohi, J. and Wereley, N. M., "Experimental characterization and static modeling of McKibben actuators," Journal of Mechanical Design, Transactions of the ASME **131**(9), 0910101–09101010 (2009).

[18] Ball, E. and Garcia, E., "Effects of bladder geometry in pneumatic artificial muscles," Journal of Medical Devices, Transactions of the ASME **10**(4) (2016).

[19] Yu, Z., Pillsbury, T., Wang, G. and Wereley, N. M., "Hyperelastic analysis of pneumatic artificial muscle with filament-wound sleeve and coated outer layer," Smart Materials and Structures **28**(10), 105019 (2019).